Journal of Medicinal Chemistry

Article

Discovery and Rational Design of Pteridin-7(8H)-one-based Inhibitors Targeting FMS-like Tyrosine Kinase 3 (FLT3) and Its Mutants

Deheng Sun, Yu Yang, Jiankun Lyu, Wei Zhou, Wenlin Song, Zhenjiang Zhao, Zhuo Chen, Yufang Xu, and Honglin Li

J. Med. Chem., **Just Accepted Manuscript** • DOI: 10.1021/acs.jmedchem.6b00374 • Publication Date (Web): 07 Jun 2016

Just Accepted

ACS Publications

Journal of Medicinal Chemistry is published by the American Chemical Society. 1155 Sixteenth Street N.W., Washington, DC 20036

Discovery and Rational Design of Pteridin-7(8*H*)-one-based Inhibitors Targeting FMS-like Tyrosine Kinase 3 (FLT3) and Its Mutants

Deheng Sun‡, Yu Yang‡, Jiankun Lyu‡, Wei Zhou, Wenlin Song, Zhenjiang Zhao, Zhuo Chen*, Yufang Xu*, and Honglin Li*

State Key Laboratory of Bioreactor Engineering, Shanghai Key Laboratory of New Drug Design, School of Pharmacy, East China University of Science & Technology, Shanghai 200237, China.

‡ Authors contributed equally to this work

* To whom correspondence should be addressed. E-mail: chenzhuo@ecust.edu.cn, yfxu@ecust.edu.cn, hlli@ecust.edu.cn

Please address requests for reprints to:

Prof. Honglin Li

School of Pharmacy, East China University of Science and Technology

130 Mei Long Road, Shanghai 200237

Phone/Fax: +86-21-64250213

Abstract

FLT3 has been validated as a therapeutic target for the treatment of acute myeloid leukemia (AML). In this paper, we describe for the first time, pteridin-7(8*H*)-one as a scaffold for potent FLT3 inhibitors derived from structural optimizations on irreversible EGFR inhibitors. The representative inhibitor (**31**) demonstrates single-digit nanomolar inhibition against FLT3, subnanomolar K_D for drug-resistance FLT3 mutants. In profiling of the *in vitro* tumor cell lines, it shows good selectivity against AML cells harboring FLT3-ITD mutations over other leukemia and solid tumor cell lines. The mechanism of action study illustrates that pteridin-7(8*H*)-one derivatives suppress the phosphorylation of FLT3 and its downstream pathways, thereby inducing G_0/G_1 cell cycle arrest and apoptosis in AML cells. In *in vivo* studies, **31** significantly suppresses the tumor growth in MV4-11 xenograft model. Overall, we provide a structurally distinct chemical scaffold with which to develop FLT3-mutants-selective inhibitors for AML treatment.

Introduction

FLT3, a member of the class III receptor tyrosine kinase family, plays a pivotal role in the development of immature hematopoietic cells.[1] Normally, through binding to its ligand, dimerization and activation of FLT3 leads to phosphorylation of downstream signaling pathways,[2] involving the Ras / mitogen-activated protein kinase (Ras/MAPK) and phosphatidylinositol 3-kinase / Akt (PI3K/Akt) pathways.[3] Mutated FLT3 however, causes constitutive ligand- independent activation of the target. Commonly, internal tandem duplication (ITD) mutations of FLT3 are harbored in approximately 30% of acute myeloid leukemia (AML) patients and are associated with poor prognosis[4-6]. FLT3-ITD mutations prefer to activate the downstream effector signal transducer and activator of transcription 5 (STAT5), which results in aberrant proliferation of leukemia cells.[7-9] In addition, subsequent point mutations in the activation loop in the FLT3 kinase domain (KD), such as D835Y, D835H, are identified as primary mechanisms of resistance to most FLT3 inhibitors which have been developed as clinical-stage drug candidates.[10] Thus, inhibition of FLT3 kinase and its mutants is a promising therapy for AML.

As FLT3 inhibitors represent a promising modality for AML treatment, discovery of novel scaffolds for selective FLT3 inhibitors has been an attractive research area in recent years.[11, 12] Several potent drug candidates have been advanced to clinic trials, including midostaurin (PKC-412),[13] lestaurtinib (CEP-701),[14] tandutinib (MLN-518),[15] sunitinib (SU11248),[16] sorafenib (BAY 43–9006),[17] quizartinib (AC220)[18] and crenolanib.[19, 20] However, the rapid development of secondary drug-resistant KD mutations of FLT3 in AML patients was found to limit the clinical

R&D of the majority of FLT3 inhibitors with the exception of crenolanib, which retains activity against ITD mutants and most resistance-conferring KD mutants of FLT3 in *in vitro* and *in vivo* models.[21, 22] Consequently, discovery of efficacious inhibitors with novel scaffolds against FLT3 and its mutants is an unmet need for AML monotherapy.

In our previous studies, the pteridin-7(8*H*)-one derivative (**1**) was identified as a highly potent irreversible inhibitor targeting epidermal growth factor receptor (EGFR) tyrosine kinases through a computational scaffold hopping protocol.[23] Recently, we unexpectedly found that **1** shows 99% and 82% inhibition of FLT3 at 10 μM and 1 μM respectively in a panel of 26 kinases (see Figure S1 in Supporting Information). However, this inhibition corresponded to only a moderate half maximal inhibitory concentration (IC_{50}) of 312 nM. We began our study of pteridin-7(8*H*)-one derived FLT3 inhibitors by analyzing the structure-activity relationships of previously synthesized pteridin-7(8*H*)-one irreversible EGFR inhibitors. Then, with the assistance of a FLT3 homology model and a subsequent docking study, we carried out a series of structural modifications on these lead compounds to improve FLT3 inhibition activities and growth inhibition potency of pteridin-7(8*H*)-ones against AML cells. Subsequently, we explored the antitumor mechanism of representative compounds in AML cell lines and investigated their kinome profiling, binding affinities for drug resistance related mutants, *in vitro* antiproliferative activities against leukemia and solid tumor cell lines, pharmacokinetics (PK) properties in rats and *in vivo* efficacy in MV4-11 tumor xenografts models. We were able to convert previously studied irreversible EGFR inhibitors into highly potent FLT3 inhibitors and

for the first time, introduce this novel and unique pteridin-7(8*H*)-one scaffold into the family of FLT3 inhibitors.

Chemistry

The pteridin-7(8*H*)-one analogues used in this study were synthesized as shown in Scheme 1. Details of the synthetic method were reported previously.[23] Condensation of commercially available 2,4-dichloro-5-nitro-pyrimidine (**I**) with a 3' or 4' -substituted arylamine in 1,4-dioxane containing N,N-diisopropylethylamine (DIPEA) gave compound **II**. Compound **III** was then obtained by nucleophilic substitution of compound **II** with a second substituted arylamine. The nitro group in **III** was reduced by hydrogenation with Pd/C in ethanol to provide **IV** containing a nucleophilic amino group in good yield. The diaminopyrimidine compound (**IV**) was cyclized with ethyl glyoxalate and acetic acid in refluxing ethanol to form the pteridin-7(8H)-one core in compound **V**. Finally, compound **V** was deprotected in trifluoroacetic acid (TFA) to generate the aminopteridin-7(8H)-ones (**VI**), which was further acylated with the corresponding acyl chloride or sulfonyl chloride to obtain the target compounds (**VII**).

Results and Discussion

Binding mode analysis.

Previously, we reported the discovery of the lead compound **1** as a potent and irreversible EGFR inhibitor. Reviewing its profile against a panel of 26 kinases, we found that it showed only moderate inhibition against FLT3. An explanation of this observation could be that the interaction modes of the lead compound with FLT3 and EGFR share a high degree of similarity (Figure 1A). The predicted binding mode shown in Figure 1A was obtained through docking the lead compound into FLT3 homology model built in an active conformation. The structure of EGFR (PDB ID: 3IKA) was aligned to the FLT3 homology model. In both structures, the aminopyrimidine ring interacts with the residue (FLT3: Cys694, EGFR: Met793) at hinge region through classical bidentate hydrogen bonding. A hydrophobic sandwich with the pteridin-7(8*H*)-one core and a floor leucine residue and a ceiling alanine residue (FLT3: Ala642 and Leu818, EGFR: Ala743 and Leu844) is formed, further stabilizing the binding interactions between lead scaffold and target. The most noticeable difference within the two inhibitor-kinase complexes is the distinct interaction between the Michael acceptor and the target. The electrophilic group forms a covalent bond with the thiol of Cys797 of EGFR, and this has been widely reported[24-27] as a vital contribution to EGFR binding affinity and selectivity. On the contrary, compound **1** binds to FLT3 noncovalently, for the corresponding location in FLT3 is occupied by a larger aspartic acid (Asp698), and the acrylamide group has to swing away from it and forms a hydrogen-bond interaction with the main chain carbonyl group of Arg815.

***In vitro* structure-activity relationship (SAR) interpretation and structural modification.**

The initial SAR analysis was based on the reported pteridin-7(8*H*)-one derivatives (compounds **1-21**, see Table 1). At first, with the same Michael acceptor group (R^2) in the 3'-position we compared the variations of R^1 on the substituted aniline at the C2 position (**1-10**). Of all these structures, the lead compound with a 4-methylpiperazinyl group (**1**) displayed the best FLT3 inhibitory activity. This experimental observation agrees significantly with the computational results. The charged 4-methylpiperazinyl group is oriented toward the solvent channel and forms a hydrogen bond with the side chain of Asn701. Absence of that interaction leads to significant loss of activity (**1** *vs* **8**), further emphasizing that a key H-bond contact in this region has a positive effect on FLT3 inhibition. Next, we turned our attention to the impact of Michael acceptors on the FLT3 potency. Comparing the compounds in pairs with the same R^1 substitution but varied Michael acceptor at the 3' or 4'-position (**1** *vs* **11**, **7** *vs* **12**, **8** *vs* **13**, **9** *vs* **14**, **10** *vs* **15**), we found that the Michael acceptor at 4'-position was more favorable for FLT3 inhibition. Increasing the length of the acrylamide fragment with the addition of a dialkylaminomethyl group (**7** *vs* **16**, **12** *vs* **17**), produced no detectable variation in FLT3 inhibition, but when the acrylamide group was replaced by a smaller amino group (**7** *vs* **18**, **12** *vs* **19**), the analogs displayed a dramatic improvement in potency. When compared with compound **7**, compound **18** showed a >50-fold enhancement in FLT3 inhibitory activity. These observations indicate that the Michael acceptor is detrimental to FLT3 inhibitory activity. In addition, the FLT3 potency decreased when group in R^3 at 2-position was methoxy (**1** *vs* **20**, **11** *vs* **21**). For new round of chemical modification, a smaller substituent could be introduced at

this position where it might eliminate a possible steric clash with the hinge region. This initial SAR analysis therefore paved the way for next round of rational lead optimization.

In the light shed by the previous docking study, new SAR explorations were devised to guide synthesis of the following analogs. A schematic representation is shown in Figure 1B. In detail, the R^1 group is a binary option (methylpiperazinyl or methoxy), while the Michael acceptor group (R^2) and R^3 group on the aniline segment are substituted with diverse groups for a second round of lead optimization.

In the new round of structural modification, R^2 substituents were investigated first. The initial SAR study suggested that removal of the Michael acceptor in R^2 should be beneficial to FLT3 inhibition. The binding mode shown in Figure 1A also implied that when the acrylamide group is converted into an amino substituent, the nearby Asp698 residue becomes accessible and available to interact with the R^2 group.

We applied this rationale to analogs bearing a 4-methylpiperazinyl group in R^1 (**1** *vs* **22**, **11** *vs* **23**). Biological testing showed 50-fold and 5-fold improvements in FLT3 inhibition, respectively supporting this hypothesis (Figure S2). The docking scores for these four compounds are also consistent with the experimental observations (Table S1 and Figure S3B). We attempted to acetylate the amino group at the 4'-position of R^2 to investigate whether the amino was crucial to the activity. When R^1 is methoxy, further substitution at the R^2 position with free amino (**19**), acetamide (**24**), or methanesulfonamide (**25**) displayed decreased FLT3 IC_{50} values of 29, 127, 255 nM,

respectively. A similar tendency was also observed with compounds **23**, **26** and **27**. These results confirmed that the exposed amino in this position is more favorable for FLT3 inhibition. Given the modeled structure of FLT3, a possible explanation is that the amino group in R^2 might form a hydrogen-bond interaction with the deprotonated carboxyl group of Asp698. If the amino group is substituted with electron withdrawing group, the strength of the favorable electrostatic interaction will be greatly diminished. Comparison of **23** with **28** (8.7 nM v.s. 37.2 nM) demonstrated that one more degree of freedom (DOF) caused by the additional methylene (Figure S4A and S4C) may increase the difficulty of maintaining optimal hydrogen bond geometries with Asp698, leading to a 4-fold loss in activity. Besides, the binding potency of compound **29** is similar with **23** (8.2 nM v.s. 8.7 nM). This is probably due to the unchanged DOF and piperazine ring's hydrogen bond with Asp698 (Figure S4B). After all, the hydrogen bond between the R^2 substituted group and the deprotonated carboxyl group of Asp698 plays an important role in FLT3 inhibition.

As was mentioned in the overall SAR, a methyl group was introduced to the 2-position in R^3 on substituted aniline at C2 position, but like the early analogs, the FLT3 potency was also reduced (**19** *vs* **30**). According to the predicted binding mode (Figure 1A), the methyl or methoxy group at 2-position should increase the possibility of a steric clash with the residues at the hinge region, such as the side-chain of Tyr693, thereby attenuating the stability of the hinge binder. However, the R^3 group at 3-position fell into a different situation. On the one hand, the hydrophobic slot formed by Leu616 and Gly697 (Figure S5) is exposed to solvent,[28] which leaves limited space for small substitutions at 3-positon in R^3. On the other hand, consistent with the

docked model (Figure 1D), introduction of a small group at the 3-position can increase the torsion angle between phenyl and 4-methylpiperazinyl ring, further stabilizing the hydrogen-bond contact between 4-methylpiperazinyl and Asn701. Moreover, it may also affect the perpendicular orientation of the two phenyl-ring system within the scaffold, leading to a favorable T-shaped intramolecular π-π stacking interaction. As expected, when the methyl or methoxy group is transferred from the 2-position (**30**) to the 3-position (**31**), the FLT3 inhibitory potency increases immediately. Compound **31** in fact displays the most potent FLT3 inhibitory effect (IC_{50} = 1.56 nM) in this series. Additionally, introduction of a halogen atom such as chlorine at this position, did not obviously decrease the FLT3 activity (**23** *vs* **33**, **19** *vs* **34**). But when a fluorine atom is placed at the 3-position, the corresponding analogues present declining potency (**23** *vs* **35)**, suggesting that strong electron-withdrawing groups are not suitable at the 3-position of R^3. All the SAR exploration at the 3-position underlines the fact that introduction of a methyl or methoxy at the 3-position in R^3 is an important contribution to improvement of the inhibitory activity against FLT3 of this series.

***In vitro* antiproliferative activities of pteridin-7(8*H*)-one derivatives.**

The antiproliferative potency of pteridin-7(8*H*)-one derivatives against selected cell lines was measured using MTT or SRB assays. The target compounds were first evaluated against the FLT3-driven AML cell line MV4-11 containing an FLT3-ITD-activating mutation. The anti-proliferative activities against MV4-11 cells of targeted compounds normally correspond with their FLT3 enzymatic inhibitory activities, ranging from 51 nM to more than 10,000 nM. Some of these were 5-times

more potent than the positive control MLN518, and comparable with the positive control AC220. Introduction of a Michael acceptor at the R^2 position leads to reduced potency. For the majority of compounds, the IC_{50} values were >1 μM in MV4-11 cell lines, further confirming that Michael acceptor is relatively unfavorable for FLT3 targeting (**1** *vs* **22**, **11** *vs* **23**). In addition, at the R^1 position, the 4-methylpiperazinyl moiety significantly contributes to cellular growth inhibition more than does a methoxy group. For example, the 4-methylpiperazinyl group-bearing derivatives **22** and **23** were 8-22 times more potent than the methoxy derivatives **18** and **19** (383 nM *vs* 3487 nM, 297 nM *vs* 6887 nM). Furthermore, the introduction of a methyl group at the R^3-position greatly enhances the antiproliferative activity. For instance, compound **31** was a 5 times more potent antiproliferative agent (51 nM *vs* 297 nM) than **23** as a result of introduction of the methyl group. Almost all the tested pteridin-7(8*H*)-one derivatives, including the potent MV4-11 growth inhibition agents, were ineffective against the FLT3-independent chronic myelogenous leukemia (CML) cell line K562. In the normal cell line WI-38, compounds such as **23** and **31**, which target FLT3 efficiently, were 33-81 fold less potent than they were in MV4-11 cells. We therefore concluded that the efficient FLT3-targeting pteridin-7(8*H*)-one derivatives exhibit selective antiproliferative activities against FLT3-driven cells rather than normal toxicity.

Inhibition of FLT3 phosphorylation and downregulation of downstream signal proteins in the MV4-11 cell line.

To investigate further whether the anti-AML activity is associated with inhibitory activation of FLT3 and its downstream signaling proteins, the representative

compound **31** was assessed and quantified by Western blot analysis (Figure 2). After 2 h treatment, **31** at a concentration of 10 nM inhibits FLT3 phosphorylation by more than 50% and down-regulates the phosphorylation of the downstream signaling proteins, AKT, ERK1/2 and STAT5 in a dose-dependent manner in MV4-11 cells, which are comparable with the known FLT3 inhibitor MLN518. The representative compound from the first round of optimization, **23** exhibits less potent inhibition of FLT3 and downstream cell signaling proteins than **31** (Figure S6), which are consistent with the SAR on the FLT3 enzymatic inhibitory activities and antiproliferative activities in MV4-11 cells.

Induction of cell cycle arrest and cell apoptosis.

Cell cycle analysis of MV4-11 cells treated with compound **31** showed dose-dependent increases in the G_0/G_1 and $subG_1$ populations, indicating both cell cycle arrest and cell death (Figure 3A). The percentage of cells in the G_0/G_1 and $subG_1$ populations increased from 70% to 86% and 0% to 12% respectively, after treatment with 100 nM of compound **31** for 48 h. As detected by Annexin V staining, a dose-dependent increase in the percentage of apoptotic and dead cells was also seen, which is consistent with the increased $subG_1$ cell population observed in MV4-11 cells treated with compound **31**. (Figure 3B). In the presence of vehicle alone for 48 h, 9% of the cells were in apoptosis. Treatment with 100 nM of compound **31** for 48 h led to an increase in the degree of apoptosis by a factor of 4.5 (40%). Remarkable cell cycle arrest and apoptosis were also observed for compound **23** at a concentration of 1000 nM (Figure S7). Accordingly, this series of pteridin-7(8*H*)-one derivatives was able to block the G_0/G_1 cell cycle, trigger apoptosis, and inhibit the growth of FLT3

mutant MV4-11 cells by modulating the FLT3 signaling pathways.

Binding affinity against wild-type and activated mutations of FLT3 Kinase.

By profiling compound **31** in a panel of 468 kinases at a concentration of 1 μM using DiscoverX's KINOMEScan technology, we identified the kinase selectivity of compound **31**. The S(10) selectivity score, which is calculated by dividing the number of nonmutant kinases which are <10% of control can be determined by the total number of nonmutant kinases. From the 403 nonmutant kinases there were 34 hits, giving a selectivity score of 0.084 (Figure 4 and Table S2, S3). Clinically relevant FLT3-resistant mutants, such as ITD, D835V, ITD/D835V are inhibited with percent control values ≤ 1%. This was further confirmed by K_D determination. As shown in Table 2, compound **31** binds wild-type FLT3 and FLT3 variants with high affinity (K_D = 0.25 - 6.9 nM). In particular, compound **31** revealed good binding affinity for drug-resistance mutants[29-34] such as D835V (K_D = 0.25 nM), ITD/D835V (K_D = 0.79 nM) and ITD/F691L (K_D = 5.7 nM). The relatively lower binding affinity of compound **23** was consistent with these results. In addition, compound **31** showed comparable binding affinity for wild-type FLT3 and FLT3-ITD mutant with AC220.

***In vitro* antiproliferative activities of compound 31 against leukemia and solid tumor cell lines.**

The antiproliferative activity of compound **31** was tested against various cell lines, including leukemia and solid tumor cell lines, and the results are listed in Table 4. Compound **31** potently inhibits the growth of AML cell lines MV4-11 and the Molm13-harboring FLT3-ITD mutant, with IC_{50} values of 51 nM and 33 nM,

respectively. It shows much weaker growth inhibition activities against leukemia RS4;11, Molt4, HL60 cells, lung cancer H1299, H1975 cells, colorectal cancer RKO, HCT116, HT29, SW620 cells, neuroblastoma SH-SY5Y cells, with IC_{50} values of 925, 2119, 1377, 4876, 4464, 1928, 2358, 3021, 2529 and 5566 nM, respectively). For other leukemia and solid tumor cell lines, including THP1, A549, DMS79, H146, H187, H209 and MCF7, compound **31** failed to exhibit a distinct growth inhibition effect at a concentration of 10,000 nM.

PK properties in rats of compound 31.

The PK properties of **31** were evaluated in rats following intravenous and oral administration (Table 3). Compound **31** was administered at a dose of 1 mg/kg in saline mixture (DMSO:PEG400:saline = 5:40:55) (iv) or 10 mg/kg in 0.5% methlcellulose (po), respectively. Its bioavailability was determined to be ≈ 26%, and the half-life of **31** was 3.1 h (iv) and 4.5 h (po). It had a volume distribution (27.69 L/kg) and clearance at 8.51 L/hr/kg.

***In vivo* Effects of 31 against MV4-11 tumor xenografts**.

The *in vivo* antitumor efficacy of compound **31** was evaluated in MV4-11 xenograft models. When the tumor grew to a mean volume of around 200 mm^3, the mice were treated orally with vehicle, 10, 25, 50 mg/kg of **31** and 10 mg/kg of AC220 once daily for 14 days. As shown in Figure 5A, **31** shown dose-dependent in vivo efficacy, with TGI = 28% ($p < 0.01$), 87% ($p < 0.001$) and 128% ($p < 0.001$) at 10, 25 and 50 mg/kg, respectively. It could induce tumor regression (TGI = 128%) upon oral administration at 50 mg/kg, which was comparable with AC220 at 10 mg/kg (TGI = 139%). No

obvious body weight changes were observed (Figure 5B). When treated with **31** intraperitoneally, significant tumor shrinkage was also induced with TGI = 129% and 136% at 25 and 50 mg/kg. ($p < 0.001$). (Figure S8) Immunohistochemical (IHC) analyses were performed to evaluate the time course of the antitumor activity of compound **31** in the MV4-11 xenograft model. As shown in Figure 5C, compound **31** (50 mg/kg/day/po) suppresses proliferation and induces late stage apoptosis in xenograft models compared with vehicle-treated tumors.

Conclusion

Guided by a docking study based on a homology model of FLT3 in an active conformation, we explored structural modifications on irreversible EGFR inhibitors. This resulted in this first report of pteridin-7(8*H*)-one derivatives acting as potent FLT3 inhibitors. In our model, the 4-methylpiperazinyl group in the R^1 substituent promotes the enzymatic and cellular activity of the compound by forming a hydrogen-bond interaction with Asn701. Conversion of the former Michael acceptor into an amino group at the 4'-position in R^2 led to a noticeable improvement in FLT3 inhibition and selectivity against FLT3 over EGFR (Table S4), because of the hydrogen-bond interaction between the amino group and Asp698. Substitution of a methyl group at the 3-position in R^3, which may further stabilize the hydrogen-bond interaction between the 4-methylpiperazinyl group and Asn701 and a favorable intramolecular π-π stacking interaction, led to compound **31**, the most potent compound in this series. This representative compound (**31**) has single-digit nanomolar FLT3 inhibitory and low-dose anti-AML activity. It shows great selectivity and significant binding affinity to FLT3 mutants in kinase profiling and growth inhibition activities against leukemia cell lines harboring FLT3-ITD mutants, MV4-11 and Molm13 over other leukemia and solid tumor cell lines in profiling of *in vitro* tumor cell lines. We also clarified the cellular cytotoxic mechanism of representative pteridin-7(8*H*)-one derived FLT3 inhibitors, which is mediated through inhibition of phosphorylation of FLT3 and downstream signaling proteins, and thereby induction of G_0/G_1 stage cell cycle arrest and apoptosis in AML cells. In the *in vivo* studies, **31** showed a long half-life [3.1 h (iv) and 4.5 h (po)] and suppressed tumor growth in the MV4-11 xenograft model in dose-dependent manner via oral administration. This

research provides a structurally distinct scaffold for development of selective FLT3 inhibitors in treatment of AML.

Experimental Section

Computational Methods

Homology modeling of an active conformation of FLT3.

The X-ray structure of FLT3 (PDB entry: 1RJB) from the Protein Data Bank (PDB, http://www.pdb.org) is in an inactive conformation, and our inhibitors cannot be docked into its ATP-binding site (Figure S10). A homology model of FLT3 was constructed in an active conformation.[22, 35] According to the results of BLAST search, the c-KIT kinase (PDB entry: 1PKG) is the highest homology kinase structure in an active conformation. This dimer of active c-KIT kinase contains two identical chains and one chain (Chain A) was selected as the structure template for homology modeling. Subsequently multiple sequence alignment (the sequence identity and similarity are 54.8% and 70.2%) and 3D structure modeling of FLT3 (Glu588-946Gln, including the KID region, which lacks a template) in an active conformation was implemented in Discovery Studio (DS) 2.5[36] with default settings. An initial homology model of FLT3 was prepared in the protein preparation wizard of Maestro[37] and subjected to energy minimization with the OPLS_2005 all-atom force field using Prime[38] in Schrödinger 2009.

The refinement of FLT3 homology model.

In order to achieve a better fit between the pteridin-7(8*H*)-one scaffold and the FLT3 homology model, the initial FLT3 model was trained by flexible docking lead compound **1**. The 3D structure of compound **1** for further docking studies was prepared using LigPrep version 2.3[39] with the Epik 2.0[40] option. Residues Leu616, Phe691, Tyr693, Leu818, Asp698 and Asn701 were defined as flexible. Induced fit

docking in Maestro version 9.0.[37] was applied for flexible docking. The induced fit docking study revealed four possible binding poses of compound **1** at the active site. We selected the model shown in Figure 1A in terms of the docking scores, and with as many reasonable interactions as possible. Then, the receptor Grids generation of the docked FLT3 homology model followed the procedures recommended by Schrödinger. The geometric center of compound **1** in the docked FLT3 homology model was defined as the box center. Compound **1** was sequentially redocked into the ATP-binding site of the model using Glide version 5.5[41] in extra precision (XP) mode with default parameters.

Then the validation of the FLT3 homology model was performed by MolProbity Ramachandran (http://kinemage.biochem.duke.edu) and Profiles-3D (DS 2.5) analysis. The Ramachandran plot (Figure S9) indicated that 91.5% of all residues were in favored regions and 100.0% of all residues were in allowed regions. The Profiles-3D analysis evaluated this FLT3 homology model with the verification score of 115.31, which was close to the expected highest score (130.55). Collectively, the FLT3 homology model we built is structurally rational.

To further validate the reliability of the FLT3 homology model built by the above procedure, three known FLT3 type I inhibitors (CEP-701, PCK-412 and Crenolanib) were docked into the receptor grid generated above respectively. The XP Gscore for CEP-701, PCK-412 and Crenolanib is -10.509, -9.370 and -9.093, respectively. The binding modes of these three inhibitors and the corresponding FLT3 IC_{50} values[18, 19] are shown in Figure S11. All inhibitors can fit the ATP-binding site of the FLT3 model well. Both CEP-701 and PCK-412 form the classical bidentate hydrogen bonds with gatekeeper+1 (Glu692) and gatekeeper+3 (Cys694) residues in the hinge region,

which is identical with the reported binding mode for the same scaffold.[42] The predicted binding mode of Crenolanib is consistent with that reported by Catherine Smith et al.[22] In addition, the more potent inhibitors CEP-701 and Crenolanib both interact with Asp698, which is the key residue for potency improvements. All the results above validates that our FLT3 homology model in an active conformation is comparatively reliable.

Molecular docking of pteridin-7(8*H*)-one compounds.

The compounds **1-35** were docked into the FLT3 homology model using the rigid docking method described above. The protonation states of the docked compounds were determined by Epik 2.0. The Gscores for all docked compounds are listed in the Table S1 and the linear relationship between Gscores and FLT3 pIC_{50} (pIC_{50} = $-\log_{10}(IC_{50})$) is shown in Figure S3. The correlation (R value) between Gscores and FLT3 pIC_{50}s for all docked compounds (including three known FLT3 inhibitors) is -0.74. This result also validates the reliability of our FLT3 homology model.

Reagents and general methods.

The general synthesis of pteridin-7(8*H*)-one compounds is described in Scheme 1 and the detailed synthetic method was reported in our previous article[23]. All compounds were purified by column chromatography using silica gel (200-300 mesh). The ^{1}H NMR spectra were recorded on a Bruker AM-400 spectrometer with chemical shift reported in ppm (in DMSO-d_6, Me_4Si as internal standard). The mass spectra were measured at the Institute of Fine Chemistry of East China University of Science and Technology. Isolated yields of the final synthetic step were calculated. Melting points

were determined using an X-6 micro-melting point apparatus. All the final compounds were tested by High Performance Liquid Chromatography and the purity in every case was >95%. The reverse phase HPLC was conducted on a Hewlett-Packard 1100 system chromatograph, which was equipped with Zorbax RX-C18 or XDB-C18 (compounds **28** and **29**) column (250 mm×4.6 mm). The mobile phase A was acetonitrile and mobile phase B was 10 mM NH_4OAc in water (pH 6.0). The gradient of 5-100% A was run at a flow rate of 1.0 mL/min over 20 min. MLN518 was obtained from Selleck Chemicals (Houston, TX, USA)

8-(3-aminophenyl)-2-((4-(4-methylpiperazin-1-yl)phenyl)amino)pteridin-7(8*H*)-one (22). Orange solid (yield 70%), mp 262.5-262.9 ^{o}C. ^{1}H NMR (400 MHz, DMSO-d_6): δ 10.01 (s, 1H), 8.81 (s, 1H), 7.99 (s, 1H), 7.35 (d, J = 7.2 Hz, 2H), 7.22 (t, J = 8.0 Hz, 1H), 6.75 (d, J = 7.2 Hz, 1H), 6.66 (br, 2H), 6.52 (br, 1H), 6.48 (d, J = 8.0 Hz, 1H), 5.35 (s, 2H), 3.02 (br, 4H), 2.46-2.44 (m, 4H), 2.23 (s, 3H). HPLC purity: 99.5%, retention time = 8.57 min. HRMS (ESI) (m/z): $[M + H]^+$ calcd for $C_{23}H_{25}N_8O$, 429.2151; found, 429.2151.

8-(4-aminophenyl)-2-((4-(4-methylpiperazin-1-yl)phenyl)amino)pteridin-7(8*H*)-one (23). Orange solid (yield 76%), mp 235.6-236.4 ^{o}C. ^{1}H NMR (400 MHz, DMSO-d_6): δ 9.98 (s, 1H), 8.79 (s, 1H), 7.99 (s, 1H), 7.33 (d, J = 6.4 Hz, 2H), 6.98 (d, J = 8.4 Hz, 2H), 6.74 (d, J = 8.4 Hz, 2H), 6.68 (br, 2H), 5.43 (s, 2H), 3.05-3.03 (m, 4H), 2.48-2.46 (m, 4H), 2.24 (s, 3H). HPLC purity: 95.4%, retention time =8.53 min. HRMS (ESI) (m/z): $[M + H]^+$ calcd for $C_{23}H_{25}N_8O$, 429.2151; found, 429.2151.

N-(4-(2-((4-methoxyphenyl)amino)-7-oxopteridin-8(7*H*)-yl)phenyl)acetamide (24). Yellow solid (yield 62%), mp > 300 °C. ^{1}H NMR (400 MHz, DMSO-d_6): δ 10.23 (s, 1H), 10.10 (s, 1H), 8.85 (s, 1H), 8.04 (s, 1H), 7.78 (d, J = 7.2 Hz, 2H), 7.34 (d, J = 7.6 Hz, 4H), 6.61 (s, 2H), 3.67 (s, 3H), 2.13 (s, 3H). HPLC purity: 97.5%, retention time =10.54 min. HRMS (ESI) (m/z): $[M + H]^+$ calcd for $C_{21}H_{19}N_6O_3$, 403.1519; found, 403.1500.

N-(4-(2-((4-methoxyphenyl)amino)-7-oxopteridin-8(7*H*)-yl)phenyl)methanesulfonamide (25). Yellow solid (yield 47%), mp > 300 °C. ^{1}H NMR (400 MHz, DMSO-d_6): δ 10.11 (br, 1H), 8.84 (s, 1H), 8.03 (s, 1H), 7.40 (s, 4H), 7.31 (br, 2H), 6.66 (br, 2H), 3.69 (s, 3H), 3.12(s, 3H). HPLC purity: 95.4%, retention time = 11.70 min. HRMS (ESI) (m/z): $[M + H]^+$ calcd for $C_{20}H_{19}N_6O_4S$, 439.1189; found, 439.1187.

N-(4-(2-((4-(4-methylpiperazin-1-yl)phenyl)amino)-7-oxopteridin-8(7*H*)-yl)phenyl)acetamide (26). Yellow solid (yield 58%), mp 288.0-288.7 °C. ^{1}H NMR (400 MHz, DMSO-d_6): δ 10.44 (s, 1H), 10.05 (s, 1H), 8.82 (s, 1H), 8.02 (s, 1H), 7.80 (d, J = 8.0 Hz, 2H), 7.32 (d, J = 8.4 Hz, 2H), 7.25 (br, 2H), 6.64 (br, 2H), 3.24 (br, 4H), 3.05 (br, 4H), 2.64 (s, 3H), 2.15 (s, 3H). HPLC purity: 97.3%, retention time = 8.17 min. HRMS (ESI) (m/z): $[M + H]^+$ calcd for $C_{25}H_{27}N_8O_2$, 471.2257; found, 471.2213.

N-(4-(2-((4-(4-methylpiperazin-1-yl)phenyl)amino)-7-oxopteridin-8(7*H*)-yl)phenyl)methanesulfonamide (27). Yellow solid (yield 50%), mp > 300 °C. ^{1}H NMR (400 MHz, DMSO-d_6): δ 10.02 (s, 1H), 8.82 (s, 1H), 8.02 (s, 1H), 7.42-7.37 (m, 4H), 7.26 (br, 2H), 6.66 (br, 2H), 3.13 (s, 3H), 3.07 (br, 4H), 2.54 (br, 4H), 2.29(s, 3H). HPLC

purity: 99.0%, retention time = 8.53 min. HRMS (ESI) (m/z): $[M + H]^+$ calcd for $C_{24}H_{27}N_8O_3S$, 507.1927; found, 507.1926.

8-(4-(aminomethyl)phenyl)-2-((4-(4-methylpiperazin-1-yl)phenyl)amino)pteridin-7(8*H*)-one (28). Yellow solid (yield 65%), mp 216.2-216.8 °C. ^{1}H NMR (400 MHz, DMSO-d_6): δ 9.99 (s, 1H), 8.82 (s, 1H), 8.01 (s, 1H), 7.55 (d, *J* = 8.0 Hz, 2H), 7.32 (d, *J* = 8.4 Hz, 2H), 7.20 (s, 2H), 6.59 (s, 2H), 3.86 (s, 2H), 3.00-2.99 (m, 4H), 2.44-2.41 (m, 4H), 2.21 (s, 3H). HPLC purity: 97.4%, retention time = 6.92 min. HRMS (ESI) (m/z): $[M + H]^+$ calcd for $C_{24}H_{27}N_8O$, 443.2308; found, 443.2304.

2-((4-(4-methylpiperazin-1-yl)phenyl)amino)-8-(4-(piperazin-1-yl)phenyl)pteridin-7(8*H*)-one (29). Yellow solid (yield 72%), mp 276.6-277.2 °C. ^{1}H NMR (400 MHz, DMSO-d_6): δ 10.01 (s, 1H), 8.81 (s, 1H), 8.00 (s, 1H), 7.26 (d, *J* = 6.8 Hz, 2H), 7.20 (d, *J* = 8.8 Hz, 2H), 7.12 (d, *J* = 8.8 Hz, 2H), 6.58 (s, 2H), 3.19-3.17 (m, 4H), 3.02-3.00 (m, 4H), 2.90-2.88 (m, 4H), 2.45-2.43 (m, 4H), 2.22 (s, 3H). HPLC purity: 98.6%, retention time = 7.86 min. HRMS (ESI) (m/z): $[M + H]^+$ calcd for $C_{27}H_{32}N_9O$, 498.2730; found, 498.2728.

8-(4-aminophenyl)-2-((4-methoxy-2-methylphenyl)amino)pteridin-7(8*H*)-one (30). Yellow solid (yield 82%), mp 149.1-149.3 °C. ^{1}H NMR (400 MHz, DMSO-d_6): δ 9.13 (s, 1H), 8.72 (s, 1H), 7.95 (s, 1H), 7.21 (s, 1H), 6.94 (d, *J* = 8.0 Hz, 2H), 6.72 (s, 1H), 6.65 (d, *J* = 8.4 Hz, 2H), 6.60 (s, 1H), 5.33 (br, 2H), 3.72 (s, 3H), 2.13 (s, 3H). HPLC purity: 96.0%, retention time =11.68 min. HRMS (ESI) (m/z): $[M + H]^+$ calcd for $C_{20}H_{19}N_6O_2$, 375.1569; found, 375.1573.

8-(4-aminophenyl)-2-((3-methyl-4-(4-methylpiperazin-1-yl)phenyl)amino)pteridin-7(8*H*)-one (31). Yellow solid (yield 74%), mp 255.6-256.3 °C. ^{1}H NMR (400 MHz, DMSO-d_6): δ 9.94 (br, 1H), 8.80 (s, 1H), 7.99 (s, 1H), 7.36 (br, 1H), 7.18 (d, *J* = 6.4 Hz, 1H), 6.97 (d, *J* = 8.4 Hz, 2H), 6.79 (d, *J* = 8.4 Hz, 1H), 6.71 (d, *J* = 8.4 Hz, 2H), 5.37 (s, 2H), 2.76-2.74 (m, 4H), 2.47 (br, 4H), 2.24 (s, 3H), 2.06 (s, 3H). HPLC purity: 99.2%, retention time = 9.44 min. HRMS (ESI) (m/z): $[M + H]^+$ calcd for $C_{24}H_{27}N_8O$, 443.2308; found, 443.2301.

8-(4-aminophenyl)-2-((3-methoxy-4-(4-methylpiperazin-1-yl)phenyl)amino)pteridin-7(8*H*)-one (32). Orange solid (yield 63%), mp 147.4-147.9 °C. ^{1}H NMR (400 MHz, DMSO-d_6): δ 9.94 (br, 1H), 8.81 (s, 1H), 7.99 (s, 1H), 7.09 (s, 2H), 6.97 (d, *J*=8.4 Hz, 2H), 6.70 (d, *J*=8.4 Hz, 2H), 6.60 (br, 1H), 5.41 (s, 2H), 3.56 (s, 3H), 2.87 (br, 4H), 2.43 (br, 4H), 2.21 (s, 3H). HPLC purity: 98.0%, retention time = 8.75 min. HRMS (ESI) (m/z): $[M + H]^+$ calcd for $C_{24}H_{27}N_8O_2$, 459.2257; found, 459.2256.

8-(4-aminophenyl)-2-((3-chloro-4-(4-methylpiperazin-1-yl)phenyl)amino)pteridin-7(8*H*)-one (33). Yellow solid (yield 62%), mp > 300 °C. ^{1}H NMR (400 MHz, DMSO-d_6): δ 10.13 (br, 1H), 8.85 (s, 1H), 8.03 (s, 1H), 7.60 (s, 1H), 7.37 (d, *J* = 7.6 Hz, 1H), 6.97 (d, *J* = 8.4 Hz, 2H), 6.89 (d, *J* = 7.6 Hz, 1H), 6.71 (d, *J* = 8.4 Hz, 2H), 5.38 (s, 2H), 2.89 (br, 4H), 2.47 (br, 4H), 2.34 (s, 3H). HPLC purity: 98.7%, retention time = 9.64 min. HRMS (ESI) (m/z): $[M + H]^+$ calcd for $C_{23}H_{24}ClN_8O$, 463.1762; found, 463.1710.

8-(4-aminophenyl)-2-((3-chloro-4-methoxyphenyl)amino)pteridin-7(8*H*)-one (34). Yellow solid (yield 75%), mp > 300 °C. ^{1}H NMR (400 MHz, DMSO-d_6): δ 10.13 (s, 1H), 8.84 (s, 1H), 8.03 (s, 1H), 7.60 (s, 1H), 7.38 (s, 1H), 6.98 (d, J = 8.4 Hz, 2H), 6.87 (s, 1H), 6.72 (d, J = 8.4 Hz, 2H), 5.39 (br, 2H), 3.79 (s, 3H). HPLC purity: 97.0%, retention time = 11.55 min. HRMS (ESI) (m/z): $[M + H]^+$ calcd for $C_{19}H_{16}ClN_6O_2$, 395.1023; found, 395.1027.

8-(4-aminophenyl)-2-((3-fluoro-4-(4-methylpiperazin-1-yl)phenyl)amino)pteridin-7(8*H*)-one (35). Yellow solid (yield 64%), mp 238.2-238.7 °C. ^{1}H NMR (400 MHz, DMSO-d_6): δ 10.13 (br, 1H), 8.84 (s, 1H), 8.02 (s, 1H), 7.32 (d, J = 12.4 Hz, 1H), 7.19 (d, J = 7.2 Hz, 1H), 6.97 (d, J = 8.4 Hz, 2H), 6.77 (br, 1H), 6.72 (d, J = 8.4 Hz, 2H), 5.39 (s, 2H), 2.92-2.90 (m, 4H), 2.45 (br, 4H), 2.22 (s, 3H).HPLC purity: 96.9%, retention time = 9.12 min. HRMS (ESI) (m/z): $[M + H]^+$ calcd for $C_{23}H_{24}FN_8O$, 447.2057; found, 447.2057.

***In Vitro* Enzymatic Activity Assay.**

The inhibitory activity of targeted compounds against FLT3 was determined using mobility shift assay by Shanghai ChemPartner Co., Ltd. Cytoplasmic FLT3 kinase contain juxtamembrane domain was provided by Carna (Cat. No. 08-154). Peptide FAM-P2 was from GL Biochem (Cat. No. 112394). Compounds were tested from 10 μM, 3-fold dilution, 7 points, in duplicate, and staurosporine was used as the reference compound. A detailed protocol description is provided in the Supporting Information.

Kinase Profiling assay and Binding Constants (K_Ds) Assay.

The kinase profiling assay and binding constants assay were conducted using the KINOMEscan platform (www.discoverx.com). Kinase-tagged T7 phage or DNA were expressed in E. coli host or HEK-293 cells. Binding reactions were assembled by kinases, liganded affinity beads and test compounds with shaking for 1 h at room temperature, then measured by qPCR. Kinome profile assays were shown as percent of control and K_D values were determined by 11-point 3-fold serial dilution of each test compound in this method. The detailed protocol description is provided in the Supporting Information.

Cell Culture.

Unless otherwise specified, cell lines were purchased from American Type Culture Collection (ATCC, Manassas, VA, USA). K562 were obtained from the Shanghai Institute of Biochemistry and Cell Biology (Shanghai, China) and were maintained in strict accordance with the supplier's instructions and established procedures.

Cell Viability Assays.

Cell proliferation was evaluated using an MTT or a SRB assay. Cancer cells were seeded into 96-well plates and cultured overnight. The cells were then treated with increasing concentrations of compounds for a further 72 h. For suspension cells (MV4-11, K562, THP1, RS4;11, Molt4, HL60, DMS79, H146, H187, H209), 20 μL (5 mg/mL in 0.9% brine) of MTT (Sigma) was added to each well. The cells were then incubated for an additional 4 h, after which 100 μL of "triplex solution" (10% SDS-5% isobutanol-12 mM HCl) was added, and the cells were incubated overnight at 37 °C. The plates were read at 570 nm on the microplate spectrophotometer

(Synergy2, BioTek). The inhibition rate on cell proliferation was calculated as: inhibition rate = (1 - $A_{570\ treated}/A_{570\ control}$) x 100%. For adherent cell lines (WI-38, A549, H1299, H1975, RKO, HCT116, HT29, SW620, SH-SY5Y, MCF7), cells were fixed with 10% trichloroacetic acid and stained with sulforhodamine B (Sigma). Sulforhodamine B in the cells was dissolved in 10 mM Tris-HCl and was measured at 515 nm using microplate spectrophotometer. The inhibition rate on cell proliferation was calculated as follows: inhibition rate = (1 - $A_{515\ treated}/A_{515\ control}$) × 100%. The IC_{50} values were obtained by the Logit method. Each experiment was repeated in triplicate.

Flow Cytometry Assays.

MV4-11 cells were seeded at a density of 1×10^5 cells/mL in six-well plates, and exposed to different concentrations of compounds. After 48 h treatment, cells were harvested and washed twice with cold PBS buffer. Cell cycle analysis follows the directions of the PI/RNase staining Solution (Tianjin Sungene Biotech). The collected cells were fixed in 70% ethanol for 1 h. Afterward, cells were stained in propidium iodide (PI) solution at room temperature in the dark for 30 min. In the Annexin-V apoptosis assay, cell samples were resuspended in binding buffer (apoptosis analysis kit from Tianjin Sungene Biotech) and incubated with Annexin-V and propidium iodide solution protected from light. The samples in both assays were analyzed using a FACS Calibur Cytometer (Becton Dickinson, San Jose, CA, USA).

Western Blot Assays.

The primary antibodies against FLT3, p-FLT3, AKT, p-AKT, STAT5, p-STAT5 and p44/42 MAPK were obtained from Cell Signaling Technology and GAPDH antibody

was from Kangchen (Shanghai, China). Cells were incubated with different concentrations of compounds. After 2 h treatment, whole-cell lysates were collected and boiled for 10 min in 2 X SDS sample buffer and subjected to SDS-PAGE. The proteins were transferred to nitrocellulose membranes (Millpore) and blocked in 5% nonfat dry milk in TBS for 1 h at room temperature and then incubated with primary antibodies, which were diluted according to product specification. The bands were visualized using HRP-conjugated secondary antibodies (Cell Signaling Technology) followed by enhanced ECL substrate (Millipore) in Tanon 5200 Multicapture System, and then quantified by ImageJ software (1.37v, National Institutes of Health, USA).

PK Analysis.

Male Sprague-Dawley rats (200-250 g) were used and randomly divided into two groups (n = 3 in each group). A catheter was surgically placed into the femoral vein for collection of blood samples. Rats were fasted overnight before dosing. Compound **31** was administered by intravenous injection or oral gavage at a dose of 1 mg/kg in saline mixture (DMSO:PEG400:saline = 5:40:55) or 10 mg/kg in 0.5% methlcellulose, respectively. Plasma of each timepoints (5 min, 15 min, 30 min, 1h, 2h, 4h, 6h, 8h, 24h) were collected into heparin tubes and compound concentrations were determined by LC-MS/MS. The LC system comprised a Waters (Waters Corporation, UAS) Ultra Performance Liquid Chromatography (UPLC) equipped with an ACQUITY UPLC binary solvent manager, ACQUITY UPLC Autosampler Mod., ACQUTIY UPLC sample organizer and ACQUITY UPLC column heater HT. Mass spectrometric analysis was performed using an API 5500 (triple-quadrupole) instrument from Applied Biosystems/MDS Sciex with an ESI Ionsource. The data acquisition and

control system were created using Analyst 1.6.2 Software from Applied Biosystems/MDS Sciex.).

***In Vivo* Efficacy for MV4-11 Xenografts.**

4-6 weeks-old BALB/c (nu/nu) mice were purchased from the Shanghai Laboratory Animal Research Center (Shanghai, China). All studies were carried out according to the Animal Care and Use Committee guidelines of China. Approximately 1×10^7 cells were implanted with a mixture of Matrigel matrix (BD Biosciences) and PBS (1:1) in a total volume of 0.1 mL/mouse. Compounds were dissolved in saline mixture (DMSO:PEG400:saline = 1:30:69). Mice were randomized into vehicle and treated groups (n = 5 for each group) to ensure equal distribution with a group mean tumor size of 0.2 cm^3. For efficacy studies, mice were dosed intraperitoneally with vehicle or with 25 and 50 mg/kg of **31** and orally with vehicle, 10, 25, 50 mg/kg of **31** and 10 mg/kg of AC220 once daily for 14 days. The average tumor volume and mice weight were measured with vernier calipers every 2 days the volume was calculated with the formula $V = (L \times W^2) / 2$, where L = length and W = width. Inhibition (%TGI) was calculated at the end of dosing period using the formula: $\%TGI = \{1 - (T_t / T_0) / (C_t / C_0)\} / (1 - C_0 / C_t)\ X\ 100$ where T_t = median tumor volume of different treatment groups at time t, T_0 = median tumor volume of different treatment groups at time 0, C_t = median tumor volume of the control group at time t and C_0 = median tumor volume of control group at time 0.

IHC staining.

After treatment of the different groups, mice MV4-11 xenografts were harvested and

fixed in formalin. Tumor samples were embedded in paraffin and prepared in sections (3 μM). Before incubation with the primary antibodies (Abcam Corporation) at room temperature, sections were deparaffinized and rehydrated, then developed in liquid 3,3'-diaminobenzidine (DAB) for 10 minutes for independent analysis. For the TUNEL assay, sections were processed according to the manufacturer's instructions from Roche Corporation.

Statistical analysis

Statistical analyses were performed with one way ANOVA followed by least significant difference post hoc analysis and t-test when compared with only two groups.

ASSOCIATED CONTENT

Supporting Information. Selectivity profile data for compound **1** versus a panel of 26 kinase targets, table and figures presenting validations of FLT3 homology model and docking results, the *in vitro* enzymatic selectivity against FLT3 over EGFR, the western blot results of compound **23** in MV4-11 cells, the cell arrest and apoptosis results of compound **23** in MV4-11 cells, *in vivo* effects of compound **31** against MV4-11 tumor xenografts via intraperitoneal administration and details of kinase selectivity of compound **31** against a panel of 468 kinases. This material is available free of charge via the Internet at http://pubs.acs.org.

AUTHOR INFORMATION

Corresponding Author

For Z. C.: Tel/Fax, +86-21- 64250213; E-mail, chenzhuo@ecust.edu.cn.

For Y. F.: Tel/Fax, +86-21- 64251399; E-mail, yfxu@ecust.edu.cn..

For H.L.: Tel/Fax: +86-21- 64250213; E-mail, hlli@ecust.edu.cn.

Author Contributions

‡These authors contributed equally.

Notes

The authors declare no competing financial interest.

ACKNOWLEDGMENT

The research was supported in part by the Fundamental Research Funds for the Central Universities, the National Natural Science Foundation of China (Grants 21302054, 81222046, 21173076 and 81230076) (Z.C., H.L.), the Shanghai

Committee of Science and Technology (Grant 14431902100, and 13ZR1453100) (Y.X., Z.C.), and the National S&T Major Project of China (Grant 2013ZX09507004), the Twelfth Five-Year National Science & Technology Support Program (grant 2012BAI29B06) and the 863 Hi-Tech Program of China (Grant 2012AA020308) (H.L.). H.L. is also sponsored by Specialized Research Fund for the Doctoral Program of Higher Education (Grant 20130074110004), the Innovation Program of Shanghai Municipal Education Commission (grant 13SG32) and Fok Ying Tung Education Foundation (Grant 141035).

ABBREVIATIONS

AML, acute myeloid leukemia; ATP, adenosine triphosphate; Cmax, maximum concentration; CLz, clearance rate; CML, chronic myelogenous leukemia; DOF, degree of freedom; DIPEA, N,N-diisopropylethylamine; EGFR, epidermal growth factor receptor; FLT3, FMS-like tyrosine kinase 3; IHC, Immunohistochemical；ITD, internal tandem duplication; KD, kinase domain; MAPK, mitogen-activated protein kinase; MTT, 3-(4,5-dimethyl-2-thiazolyl)-2,5-diphenyl-2-H-tetrazolium bromide; PDB, Protein Data Bank; p-FLT3/p-ERK/p-STAT5/p-AKT, phosphorylated FLT3/ERK/STAT5/AKT; PI3K, phosphatidylinositol 3-kinase; R&D, research and development; SAR, structure-activity relationship; SRB, Sulforhodamine B; STAT5, signal transducer and activator of transcription 5; TFA, trifluoroacetic acid; Vss, the steady-state volume of distribution.

REFERENCE

(1) Stirewalt, D. L.; Radich, J. P. The role of FLT3 in haematopoietic malignancies. *Nat. Rev. Cancer* **2003**, *3*, 650-665.

(2) Drexler, H. Expression of FLT3 receptor and response to FLT3 ligand by leukemic cells. *Leukemia* **1996**, *10*, 588-599.

(3) Takahashi, S. Downstream molecular pathways of FLT3 in the pathogenesis of acute myeloid leukemia: biology and therapeutic implications. *J. Hematol. Oncol.* **2011**, *4*, 1-10.

(4) Network, C. G. A. R. Genomic and epigenomic landscapes of adult de novo acute myeloid leukemia. *N. Engl. J. Med.* **2013**, *368*, 2059.

(5) Quentmeier, H.; Reinhardt, J.; Zaborski, M.; Drexler, H. FLT3 mutations in acute myeloid leukemia cell lines. *Leukemia* **2003**, *17*, 120-124.

(6) Leung, A.; Man, C.; Kwong, Y. FLT3 inhibition: a moving and evolving target in acute myeloid leukemia. *Leukemia* **2012**, *27*, 260-268.

(7) Choudhary, C.; Schwäble, J.; Brandts, C.; Tickenbrock, L.; Sargin, B.; Kindler, T.; Fischer, T.; Berdel, W. E.; Müller-Tidow, C.; Serve, H. AML-associated Flt3 kinase domain mutations show signal transduction differences compared with Flt3 ITD mutations. *Blood* **2005**, *106*, 265-273.

(8) Tse, K. F.; Mukherjee, G.; Small, D. Constitutive activation of FLT3 stimulates multiple intracellular signal transducers and results in transformation. *Leukemia* **2000**, *14*, 1766-1776.

(9) Hayakawa, F.; Towatari, M.; Kiyoi, H.; Tanimoto, M.; Kitamura, T.; Saito, H.; Naoe, T. Tandem-duplicated Flt3 constitutively activates STAT5 and MAP kinase and

introduces autonomous cell growth in IL-3-dependent cell lines. *Oncogene* **2000**, *19*, 624-631.

(10) Smith, C. C.; Wang, Q.; Chin, C.-S.; Salerno, S.; Damon, L. E.; Levis, M. J.; Perl, A. E.; Travers, K. J.; Wang, S.; Hunt, J. P. Validation of ITD mutations in FLT3 as a therapeutic target in human acute myeloid leukemia. *Nature* **2012**, *485*, 260-263.

(11) Swords, R.; Freeman, C.; Giles, F. Targeting the FMS-like tyrosine kinase 3 in acute myeloid leukemia. *Leukemia* **2012**, *26*, 2176-2185.

(12) Sudhindra, A.; Smith, C. C. FLT3 Inhibitors in AML: Are We There Yet? *Curr. Hematol. Malig. Rep.* **2014**, *9*, 174-185.

(13) Stone, R. M.; Fischer, T.; Paquette, R.; Schiller, G.; Schiffer, C. A.; Ehninger, G.; Cortes, J.; Kantarjian, H. M.; DeAngelo, D. J.; Huntsman-Labed, A. Phase IB study of the FLT3 kinase inhibitor midostaurin with chemotherapy in younger newly diagnosed adult patients with acute myeloid leukemia. *Leukemia* **2012**, *26*, 2061-2068.

(14) Levis, M.; Ravandi, F.; Wang, E. S.; Baer, M. R.; Perl, A.; Coutre, S.; Erba, H.; Stuart, R. K.; Baccarani, M.; Cripe, L. D. Results from a randomized trial of salvage chemotherapy followed by lestaurtinib for patients with FLT3 mutant AML in first relapse. *Blood* **2011**, *117*, 3294-3301.

(15) DeAngelo, D. J.; Stone, R. M.; Heaney, M. L.; Nimer, S. D.; Paquette, R. L.; Klisovic, R. B.; Caligiuri, M. A.; Cooper, M. R.; Lecerf, J.-M.; Karol, M. D. Phase 1 clinical results with tandutinib (MLN518), a novel FLT3 antagonist, in patients with acute myelogenous leukemia or high-risk myelodysplastic syndrome: safety, pharmacokinetics, and pharmacodynamics. *Blood* **2006**, *108*, 3674-3681.

(16) Pratz, K. W.; Cortes, J.; Roboz, G. J.; Rao, N.; Arowojolu, O.; Stine, A.;

Shiotsu, Y.; Shudo, A.; Akinaga, S.; Small, D. A pharmacodynamic study of the FLT3 inhibitor KW-2449 yields insight into the basis for clinical response. *Blood* **2009**, *113*, 3938-3946.

(17) Ravandi, F.; Alattar, M. L.; Grunwald, M. R.; Rudek, M. A.; Rajkhowa, T.; Richie, M. A.; Pierce, S.; Daver, N.; Garcia-Manero, G.; Faderl, S. Phase 2 study of azacytidine plus sorafenib in patients with acute myeloid leukemia and FLT-3 internal tandem duplication mutation. *Blood* **2013**, *121*, 4655-4662.

(18) Zarrinkar, P. P.; Gunawardane, R. N.; Cramer, M. D.; Gardner, M. F.; Brigham, D.; Belli, B.; Karaman, M. W.; Pratz, K. W.; Pallares, G.; Chao, Q. AC220 is a uniquely potent and selective inhibitor of FLT3 for the treatment of acute myeloid leukemia (AML). *Blood* **2009**, *114*, 2984-2992.

(19) Galanis, A.; Ma, H.; Rajkhowa, T.; Ramachandran, A.; Small, D.; Cortes, J.; Levis, M. Crenolanib is a potent inhibitor of FLT3 with activity against resistance-conferring point mutants. *Blood* **2014**, *123*, 94-100.

(20) Zimmerman, E. I.; Turner, D. C.; Buaboonnam, J.; Hu, S.; Orwick, S.; Roberts, M. S.; Janke, L. J.; Ramachandran, A.; Stewart, C. F.; Inaba, H. Crenolanib is active against models of drug-resistant FLT3-ITD− positive acute myeloid leukemia. *Blood* **2013**, *122*, 3607-3615.

(21) Grunwald, M. R.; Levis, M. J. FLT3 inhibitors for acute myeloid leukemia: a review of their efficacy and mechanisms of resistance. *Int. J. Hematol.* **2013**, *97*, 683-694.

(22) Smith, C. C.; Lasater, E. A.; Lin, K. C.; Wang, Q.; McCreery, M. Q.; Stewart, W. K.; Damon, L. E.; Perl, A. E.; Jeschke, G. R.; Sugita, M. Crenolanib is a selective type I pan-FLT3 inhibitor. *Proc. Natl. Acad. Sci.* **2014**, *111*, 5319-5324.

(23) Zhou, W.; Liu, X.; Tu, Z.; Zhang, L.; Ku, X.; Bai, F.; Zhao, Z.; Xu, Y.; Ding, K.; Li, H. Discovery of Pteridin-7 (8 H)-one-based irreversible inhibitors targeting the epidermal growth factor receptor (EGFR) Kinase T790M/L858R mutant. *J. Med. Chem.* **2013**, *56*, 7821-7837.

(24) Zhou, W.; Ercan, D.; Chen, L.; Yun, C.-H.; Li, D.; Capelletti, M.; Cortot, A. B.; Chirieac, L.; Iacob, R. E.; Padera, R. Novel mutant-selective EGFR kinase inhibitors against EGFR T790M. *Nature* **2009**, *462*, 1070-1074.

(25) Song, Z.; Ge, Y.; Wang, C.; Huang, S.; Shu, X.; Liu, K.; Zhou, Y.; Ma, X. Challenges and Perspectives on the Development of Small-molecule EGFR Inhibitors against T790M-mediated Resistance in Non-small-cell Lung Cancer. *J. Med. Chem.* **2016**.

(26) Walter, A. O.; Sjin, R. T. T.; Haringsma, H. J.; Ohashi, K.; Sun, J.; Lee, K.; Dubrovskiy, A.; Labenski, M.; Zhu, Z.; Wang, Z. Discovery of a mutant-selective covalent inhibitor of EGFR that overcomes T790M-mediated resistance in NSCLC. *Cancer Discov.* **2013**, *3*, 1404-1415.

(27) Cross, D. A.; Ashton, S. E.; Ghiorghiu, S.; Eberlein, C.; Nebhan, C. A.; Spitzler, P. J.; Orme, J. P.; Finlay, M. R. V.; Ward, R. A.; Mellor, M. J. AZD9291, an irreversible EGFR TKI, overcomes T790M-mediated resistance to EGFR inhibitors in lung cancer. *Cancer Discov.* **2014**, *4*, 1046-1061.

(28) Furet, P.; Bold, G.; Meyer, T.; Roesel, J.; Guagnano, V. Aromatic interactions with phenylalanine 691 and cysteine 828: a concept for FMS-like tyrosine kinase-3 inhibition. Application to the discovery of a new class of potential antileukemia agents. *J. Med. Chem.* **2006**, *49*, 4451-4454.

(29) Williams, A. B.; Nguyen, B.; Li, L.; Brown, P.; Levis, M.; Leahy, D.; Small,

D. Mutations of FLT3/ITD confer resistance to multiple tyrosine kinase inhibitors. *Leukemia* **2013**, *27*, 48-55.

(30) Albers, C.; Leischner, H.; Verbeek, M.; Yu, C.; Illert, A. L.; Peschel, C.; von Bubnoff, N.; Duyster, J. The secondary FLT3-ITD F691L mutation induces resistance to AC220 in FLT3-ITD+ AML but retains in vitro sensitivity to PKC412 and Sunitinib. *Leukemia* **2013**, *27*, 1416-1418.

(31) Barry, E. V.; Clark, J. J.; Cools, J.; Roesel, J.; Gilliland, D. G. Uniform sensitivity of FLT3 activation loop mutants to the tyrosine kinase inhibitor midostaurin. *Blood* **2007**, *110*, 4476-4479.

(32) Gilliland, D. G. FLT3-activating mutations in acute promyelocytic leukemia: a rationale for risk-adapted therapy with FLT3 inhibitors. *Best Practice & Research Clinical Haematology* **2003**, *16*, 409-417.

(33) Moore, A. S.; Faisal, A.; de Castro, D. G.; Bavetsias, V.; Sun, C.; Atrash, B.; Valenti, M.; de Haven Brandon, A.; Avery, S.; Mair, D. Selective FLT3 inhibition of FLT3-ITD+ acute myeloid leukemia resulting in secondary D835Y mutation: a model for emerging clinical resistance patterns. *Leukemia* **2012**, *26*, 1462-1470.

(34) Yamamoto, Y.; Kiyoi, H.; Nakano, Y.; Suzuki, R.; Kodera, Y.; Miyawaki, S.; Asou, N.; Kuriyama, K.; Yagasaki, F.; Shimazaki, C. Activating mutation of D835 within the activation loop of FLT3 in human hematologic malignancies. *Blood* **2001**, *97*, 2434-2439.

(35) Li, Z.; Wang, X.; Eksterowicz, J.; Gribble Jr, M. W.; Alba, G. Q.; Ayres, M.; Carlson, T. J.; Chen, A.; Chen, X.; Cho, R. Discovery of AMG 925, a FLT3 and CDK4 Dual Kinase Inhibitor with Preferential Affinity for the Activated State of FLT3. *J. Med. Chem.* **2014**, *57*, 3430-3449.

(36) Discovery Studio, version 2.5; Accelrys, Inc.: San Diego, CA, 2009.

(37) Maestro, version 9.0; Schrödinger, LLC: New York, NY, 2009.

(38) Prime, version 2.1; Schrödinger, LLC: New York, NY, 2009.

(39) LigPrep, version 2.3; Schrödinger, LLC: New York, NY, 2009.

(40) Epik, version 2.0; Schrödinger, LLC: New York, NY, 2009.

(41) Glide, version 5.5; Schrödinger, LLC: New York, NY, 2009.

(42) Ghose, A. K.; Herbertz, T.; Pippin, D. A.; Salvino, J. M.; Mallamo, J. P. Knowledge based prediction of ligand binding modes and rational inhibitor design for kinase drug discovery. *J. Med. Chem.* **2008**, *51*, 5149-5171.

Figure Captions

Figure 1. (A) Compound **1** at the active site of the FLT3 homology model (template PDB ID: 1PKG) with the P-loop hidden for clarity. The green-colored compound **1** is presented as a ball and stick model. The contacting residues in the active site are depicted as stick and the backbone of hinge region is shown as stick. The EGFR crystal structure (PDB ID: 3IKA) is aligned to the homology model of FLT3 and residues in EGFR are highlighted in pink stick presentation. (B) SAR overview. (C) The FLT3 inhibition IC_{50} curves of compound **1** and **31** (D) Compound **31** docked into the active site of the FLT3 homology model with the P-loop hidden for clarity.

Figure 2. Western blot analysis. (A) Compound **31** inhibits FLT3 auto-phosphorylation and the phosphorylation of downstream signaling effectors STAT5, ERK and AKT in 2 h. (B) Immunoblots quantification of p-FLT3, p-STAT5, p-AKT and p-ERK, respectively. All bands were quantified and normalized by GAPDH. The data are expressed as mean ± SEM from at least three independent experiments.

Figure 3. After 48 h treatment, compound **31** induces dose-dependent cell cycle G_0/G_1 phase arrest (A) and apoptosis (B) in MV4-11 cells.

Figure 4. Profiling of compound **31** at a 1 μM concentration versus a panel of 468 kinase targets. The blue circles label the FLT3 and its related mutants. The red circles label the off-targets. FLT3, 5 main FLT3-related mutants and 7 main off-targets (inhibition with percent control values ≤ 1%) are labeled in bold font style.

Figure 5. *In vivo* effects of compound **31** against MV4-11 tumor xenografts via oral administration. (A) Compound **31** and AC220 were administered orally at concentrations ranging from 10 to 50 mg/kg/d. N = 5 for each group. Data are shown as mean ± SEM. (B) Body weight change in mouse xenograft model for each daily dosing group. (C) After 1 and 3 days of compound **31** once daily oral treatment, Ki67 and TUNEL were detected in MV4-11 tumors (three per group).

Tables

Table 1. *In vitro* enzymatic inhibitory and cellular antiproliferative activities of Pteridin-7(8*H*)-one compounds.

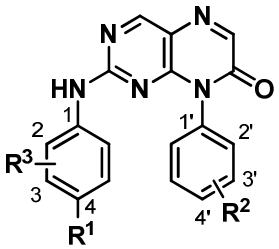

Comp.	R^1	R^2	R^3	*In vitro* Enzyme FLT3 Inhibitory Activity (IC_{50}, nM)	Cellular anti-proliferative activity (IC_{50}, nM)		
					MV4-11[a]	K562[b]	WI-38[c]
1		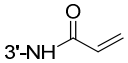	H	312 ± 15	792 ± 182	>10,000	>10,000
2		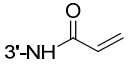	H	1528 ± 627	>10,000	>10,000	>10,000

3		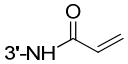	H	1056 ± 251	5559 ± 1130	>10,000	>10,000
4		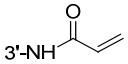	H	1747 ± 14	>10,000	>10,000	>10,000
5	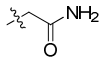	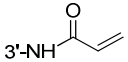	H	2958 ± 1649	>10,000	>10,000	>10,000
6	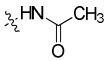	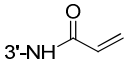	H	5449 ± 2688	7384 ± 1732	>10,000	>10,000
7	OMe	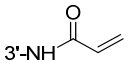	H	1869 ± 393	2611 ± 798	>10,000	8710 ± 1137
8	H	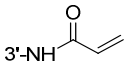	H	2920 ± 1501	5509 ± 1557	>10,000	>10,000
9	Cl	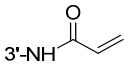	H	3589 ± 1080	4035 ± 903	>10,000	>10,000

10		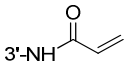	H	1136 ± 477	>10,000	>10,000	>10,000
11		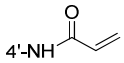	H	47 ± 6	835 ± 108	>10,000	>10,000
12	OMe	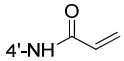	H	108 ± 28	3812 ± 1347	>10,000	>10,000
13	H	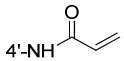	H	165 ± 52	>10,000	>10,000	>10,000
14	Cl	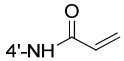	H	384 ± 37	>10,000	>10,000	>10,000
15		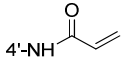	H	173 ± 51	3489 ± 1235	>10,000	>10,000
16	OMe	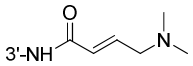	H	4413 ± 36	2721 ± 1086	>10,000	>10,000

17	OMe	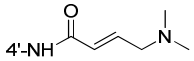	H	184 ± 45	2170 ± 938	>10,000	>10,000
18	OMe	3'-NH_2	H	34 ± 6	3487 ± 2068	>10,000	>10,000
19	OMe	4'-NH_2	H	29 ± 2	6887 ± 2042	>10,000	>10,000
20		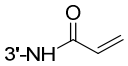	2-OMe	1317 ± 209	2887 ± 1143	>10,000	8236 ± 1854
21		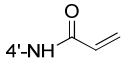	2-OMe	153 ± 38	814 ± 159	>10,000	>10,000
22		3'-NH_2	H	6.13 ± 0.53	383 ± 129	>10,000	>10,000
23		4'-NH_2	H	8.74 ± 1.08	297 ± 93	>10,000	>10,000

24	OMe	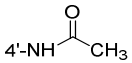	H	127 ± 35	3882 ± 1526	>10,000	>10,000
25	OMe	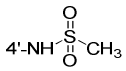	H	255 ± 83	2943 ± 1131	>10,000	>10,000
26		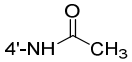	H	22.2 ± 5.13	415 ± 89	>10,000	>10,000
27		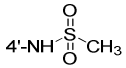	H	32.0 ± 13.5	1154 ± 501	>10,000	>10,000
28		4'-CH_2NH_2	H	37.2 ± 3.6	326 ± 49	9958 ± 369	>10,000
29		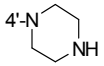	H	8.2 ± 3.7	168 ± 57	>10,000	>10,000
30	OMe	4'-NH_2	2-Me	347 ± 71	6037 ± 1670	>10,000	>10,000

31		4'-NH_2	3-Me	1.56 ± 0.06	51 ± 9	>10,000	4124 ± 386
32		4'-NH_2	3-OMe	3.19 ± 1.04	93 ± 7	>10,000	>10,000
33		4'-NH_2	3-Cl	5.24 ± 0.04	98 ± 39	>10,000	3492 ± 578
34	OMe	4'-NH_2	3-Cl	27.7 ± 1.6	1949 ± 451	>10,000	>10,000
35		4'-NH_2	3-F	35.8 ± 3.9	1417 ± 857	>10,000	>10,000
AC220	--	--	--	4.2 ± 0.3[d]	26 ± 12	>10,000	>10,000
MLN518	--	--	--	220[e]	302 ± 95	>10,000	>10,000

Staurosporine	--	--	--	0.2 ± 0.02	n.d.[f]	n.d.	n.d.

Data are averages of at least three independent determinations and reported as the means ± SDs (standard deviations).

[a.] MV4-11, cell lines harboring FLT3-ITD mutation and characterized by a ligand-independent FLT3 receptor activation.

[b.] K562, chronic myeloid leukemia cell lines without FLT3 expression.

[c.] WI-38, normal embryonic lung tissue cell lines.

[d.] Data from *Blood* **2009**, *114* (14): 2984-2992.

[e.] Data from *Cancer Cell* **2002**, 1(5): 421-432.

[f.] Not determined.

Table 2. Binding affinity to wild-type and mutant FLT3 of compounds **23, 31** and AC220.

Comp.	Binding affinity (K_D, nM)							
	Wild type	ITD	D835H	D835Y	D835V	ITD/D835V	ITD/F691L	Autoinhibited
23	75	270	44	32	n.d.[a]	n.d.[a]	n.d.[a]	n.d.[a]
31	5	6.9	1.8	2	0.25	0.79	5.7	79
AC220[b]	1.3	8.8	3.7	7.1	n.d.[a]	n.d.[a]	n.d.[a]	n.d.[a]

[a] Not determined

[b] Data from supporting information of *Nat. Biotechnol.* **2011**, 29(11): 1046-1051.

Table 3. PK properties of compound **31** in rats.

(A) Intravenous Administration					
dose (mg/kg)	C_{max} (ng/mL)	Cl (L hr^{-1} kg^{-1})	V_{ss} (L/kg)	$t_{1/2}$ (h)	$AUC_{(0-\infty)}$ (ng·h/mL)
1	55.23 ± 9.80	8.51 ± 1.07	27.69 ± 6.72	3.11 ± 1.2	118.72 ± 13.93

(B) Oral Administration					
dose (mg/kg)	t_{max} (h)	C_{max} (ng/mL)	$t_{1/2}$ (h)	$AUC_{(0-\infty)}$ (ng·h/mL)	F (%)
10	2.17 ± 1.76	40.98 ± 17.79	4.49 ± 3.35	311.11 ± 49.23	26.42 ± 4.69

Data are averages of three independent determinations and reported as the means ± SDs (standard deviations).

Table 4. Antiproliferative activity of compound **31** against various cell lines.

Cancer type	cell line	IC_{50} (nM)
acute myeloid leukemia	MV4-11	51 ± 9
acute myeloid leukemia	Molm13	32.9 ± 0.5
acute monocytic leukemia	THP1	> 10,000
acute lymphoblastic leukemia	RS4;11	925 ± 224
acute lymphoblastic leukemia	Molt4	2119 ± 76
acute promyelocytic leukemia	HL60	1377 ± 326
small cell lung cancer	DMS79	> 10,000
small cell lung cancer	H146	> 10,000
small cell lung cancer	H187	> 10,000
small cell lung cancer	H209	> 10,000
lung carcinoma	A549	> 10,000
non-small cell lung cancer	H1299	4876 ± 1329
non-small cell lung cancer	H1975	4464 ± 1645
colon carcinoma	RKO	1928 ± 869
colorectal carcinoma	HCT116	2358 ± 224
colorectal adenocarcinoma	HT29	3021 ± 801
colorectal adenocarcinoma	SW620	2529 ± 271
neuroblastoma	SH-SY5Y	5566 ± 176
breast adenocarcinoma	MCF7	> 10,000

Data are averages of at least three independent determinations and reported as the means ± SDs (standard deviations).

Scheme 1. Synthesis of pteridin-7(8*H*)-one derivatives

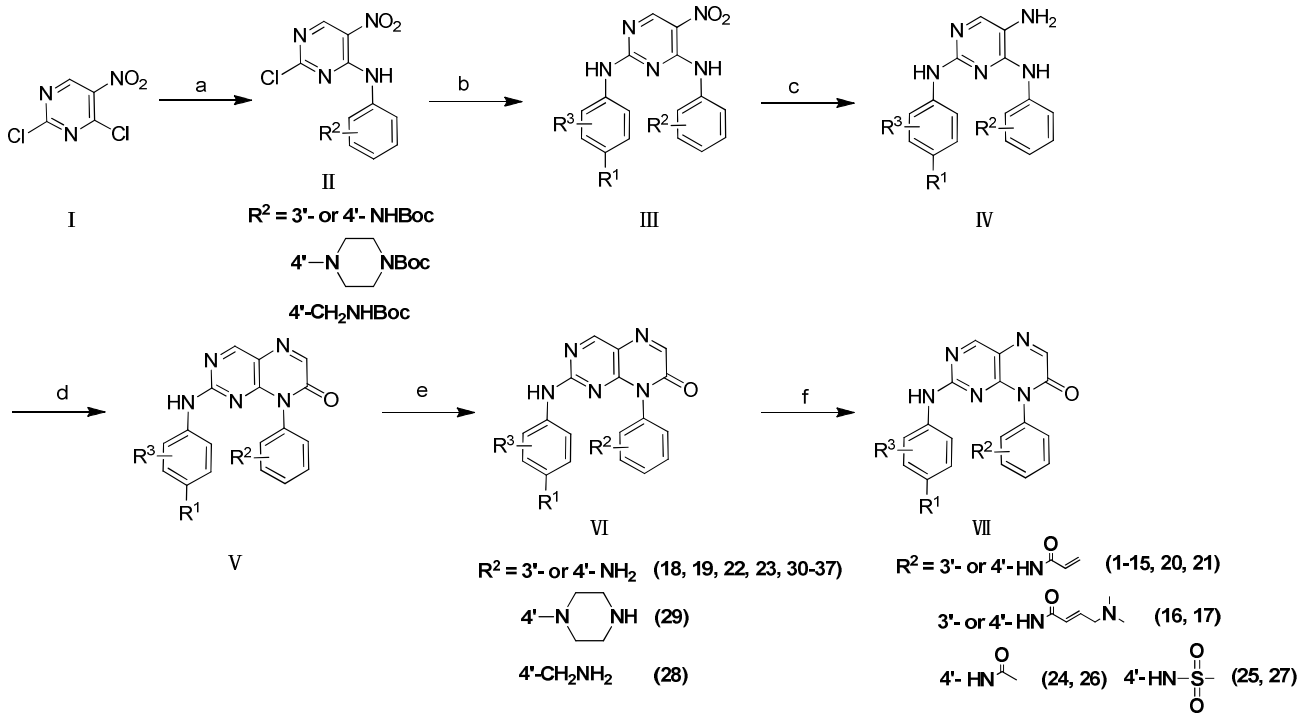

[a]Reagent and conditions：(a) $ArNH_2$, DIPEA, 1,4-dioxane, r.t.; (b) $ArNH_2$, DIPEA, 1,4-dioxane, r.t.; (c) Pd/C, H_2, EtOH; (d) EtOOC-CHO, HOAc, EtOH, reflux; (e) TFA, CH_2Cl_2, 0 ^oC to r.t.; (f) acyl chloride, Et_3N, CH_2Cl_2, 0 ^oC to r.t. or CH_3SO_2Cl, 1-methyl-2-pyrrolidinone, CH_3CN, 0 ^oC to r.t..

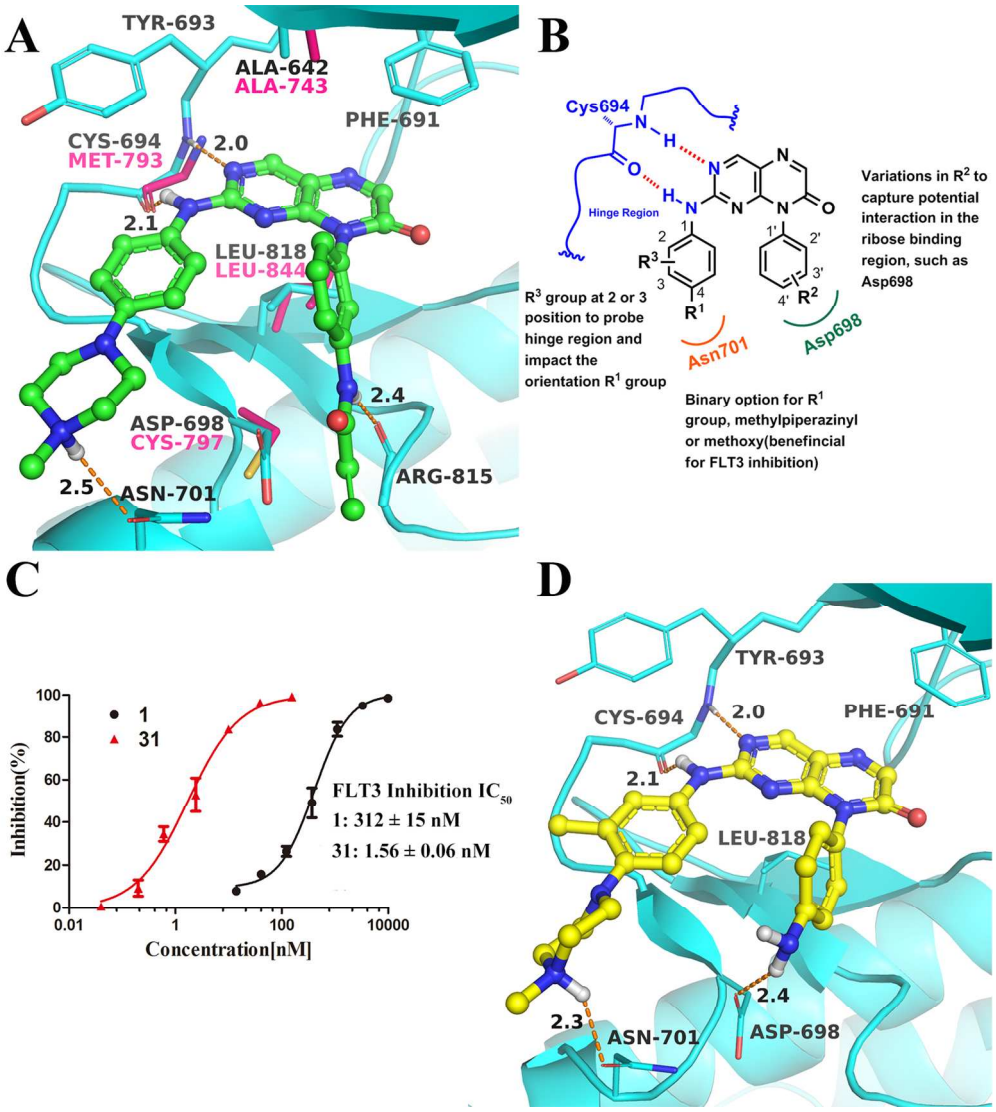

Figure 1. Structure-activity relationship
140x154mm (300 x 300 DPI)

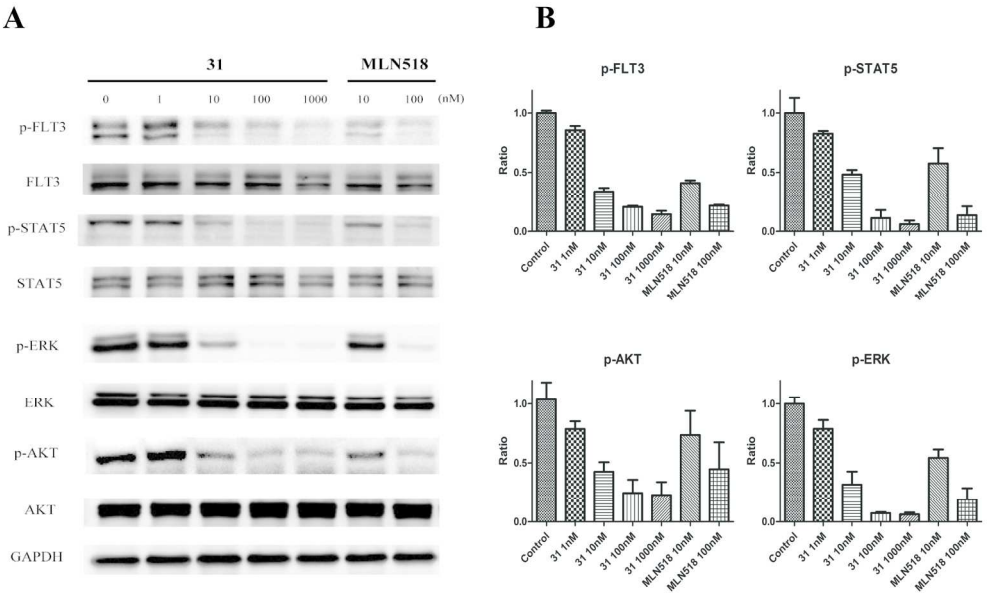

Figure 2. Western blot analysis
179x109mm (300 x 300 DPI)

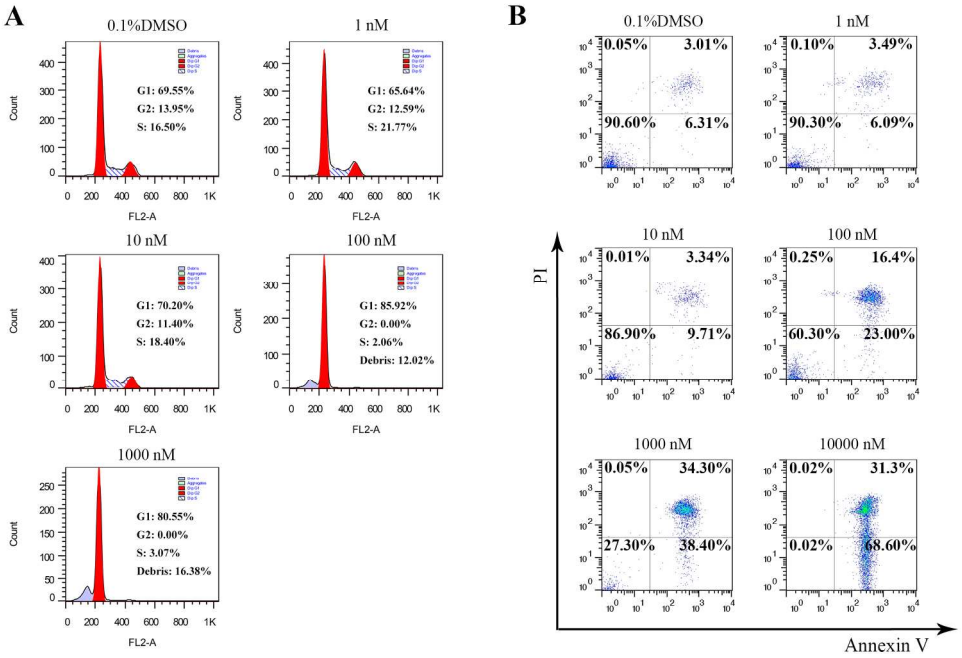

Figure 3. Drug induced Cell cycle arrest and apoptosis
199x136mm (300 x 300 DPI)

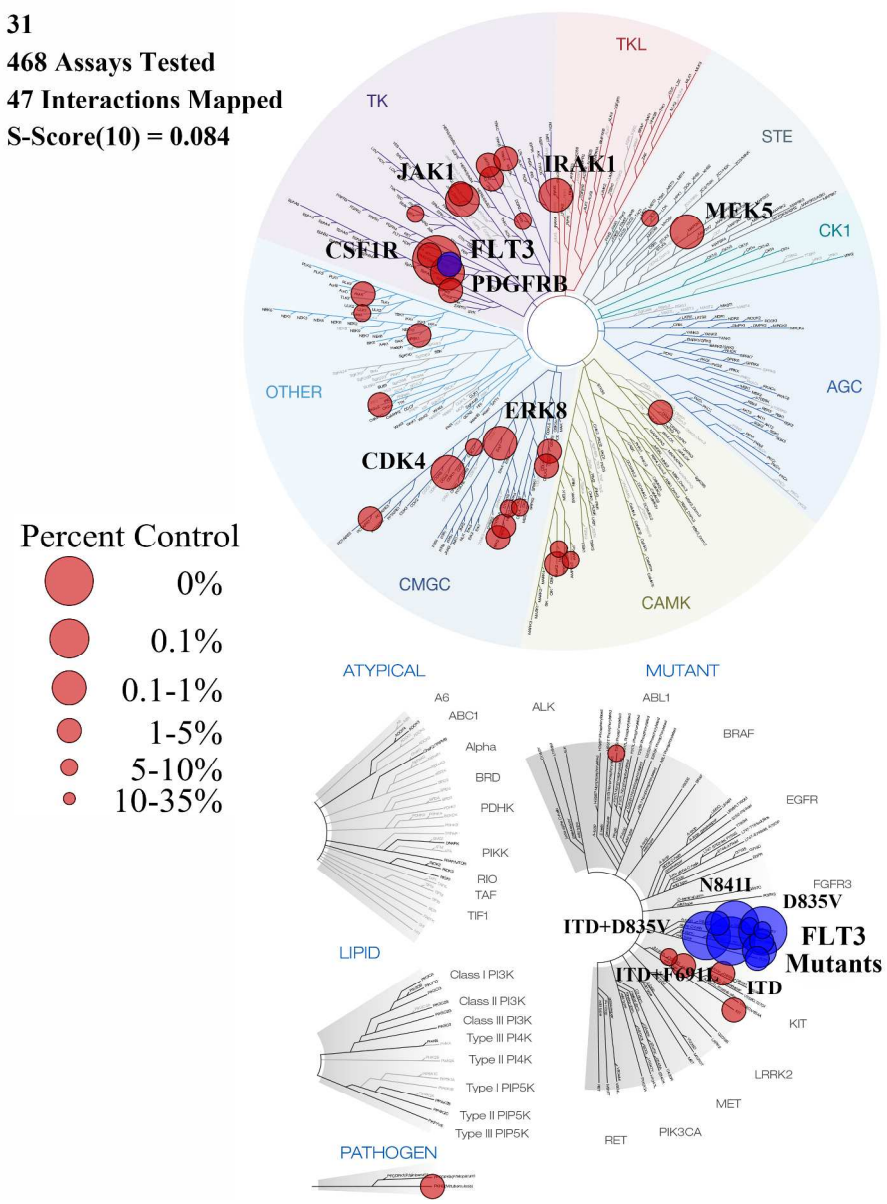

Figure 4. Kinase profiling
947x1250mm (72 x 72 DPI)

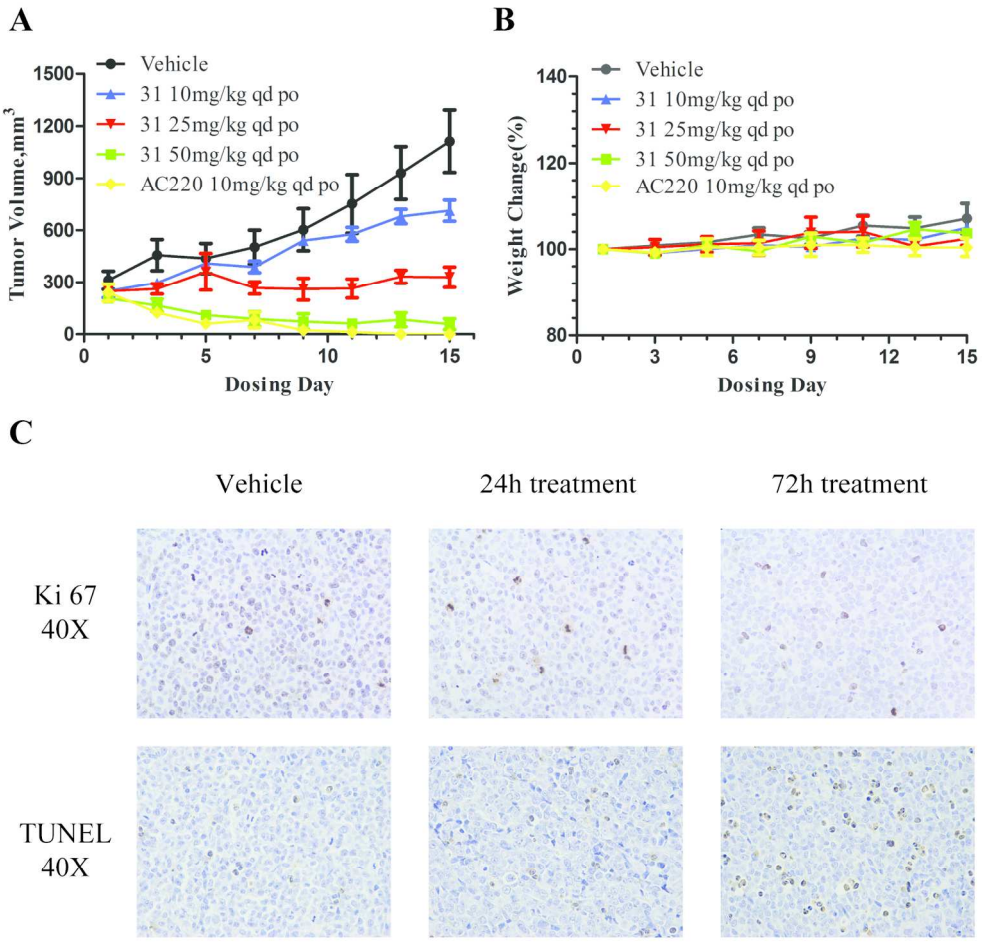

Figure 5. In vivo efficacy
165x160mm (300 x 300 DPI)

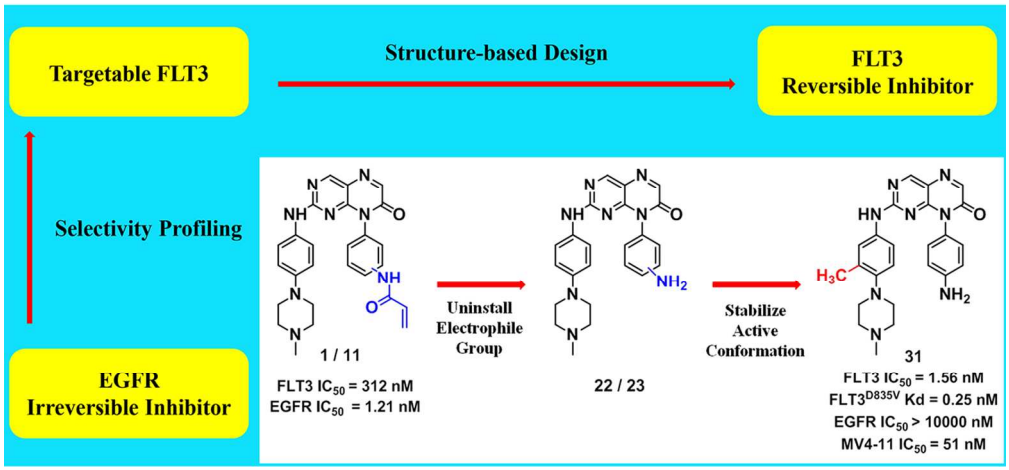

Table of Contents Graphic
119x55mm (300 x 300 DPI)